

Control of the vortex lattice formation in coupled atom-molecular Bose-Einstein condensate in a double well potential: Role of atom-molecule coupling, trap rotation frequency and detuning parameter

Moumita Gupta¹ and Krishna Rai Dastidar^{2,*}

¹Charuchandra College, Kolkata-700029, INDIA

²Indian Association for the Cultivation of Science, Kolkata-700032, INDIA

* spkrd@iacs.res.in

Abstract

We study the vortex formation in coupled atomic and molecular condensates in a rotating double well trap by numerically solving the coupled Gross-Pitaevskii like equations. Starting with the atomic condensate in the double well potential we considered two-photon Raman photo-association for coherent conversion of atoms to molecules. It is shown that the competition between atom-molecule coupling strength and repulsive atom-molecule interaction controls the spacings between atomic and molecular vortices and the rotation frequency of the trap is the key player for controlling the number of visible atomic and molecular vortices. Whereas the Raman detuning controls the spacing between atomic and molecular vortices as well as the number of atomic and molecular vortices in the trap. We have shown by considering the molecular lattices the distance between two molecular vortices can be controlled by varying the Raman detuning. In addition we have found that the Feynman rule relating the total number of vortices and average angular momentum both for atoms and molecules can be satisfied by considering the atomic and molecular vortices those are hidden in density distribution and seen as singularities in phase distribution of the coupled system except for the lattice structure where molecular vortices are overlapped with each other. It is found that although the number of visible/core vortices in atomic and molecular vortex lattices depends significantly on the system parameters the number of atomic and molecular hidden vortices remains constant in most of the cases.

1 Introduction

Realization of molecular Bose-Einstein condensate (BEC) via two-photon Raman photoassociation [1, 2, 3] and magnetic Feshbach resonance [4] has led to a

plethora of theoretical and experimental studies in the coupled atomic-molecular system [5, 6, 7, 8, 9, 10]. Coherent conversion of an atomic BEC to a molecular BEC via two-photon Raman photoassociation is important to study the quantum superchemistry of the system [7, 8, 11]. This coupled atomic-molecular BEC is also an interesting system to study the vortex lattices which has not been much explored. Formation of quantized vortices as well as highly ordered vortex lattices by rapidly rotating the trapping potential is one of the distinct characteristics of BEC which is a signature of superfluidity [12, 13]. For higher values of rotation frequencies the vortex lattice structure can be observed. The detailed dynamics of vortex lattice formation of an atomic BEC in a rotating harmonic potential has been studied [14, 15]. The influence of dipole-dipole interaction on the formation and stability of atomic vortex lattice structure has been also demonstrated [16, 17]. Ground state vortex properties have been investigated in two-component BEC [18] and vortex lattice pattern has been emerged in two-component mixture of ^{85}Rb - ^{133}Cs [19]. Formation of quantized ring vortices in coupled atom-molecular BEC of ^{87}Rb atoms trapped in a rotating three dimensional anisotropic cylindrical trap has been investigated and the stability of these atomic and molecular vortices has been examined [20]. A vortex molecule has been predicted in rotating two-component BEC whose internal states are coherently coupled [21] and stable vortex structure of molecules have been also studied in multicomponent BECs [22]. Vortex lattices has been found in a rotating atomic-molecular BEC by Woo et al and the coherent coupling between the atoms and molecules gives a pairing between atomic and molecular vortices like a carbon-di-oxide molecule [23]. Controlling atom-molecule interaction and Raman detuning parameter formation of vortex lattice structure in rotating atomic molecular BECs could be changed from overlapped atomic-molecular to carbon-di-oxide type [24].

The theoretical and experimental studies of vortices and vortex lattice structure in atomic BECs, two-component BECs or coherently coupled atomic-molecular BECs described so far are for the system which is trapped inside single harmonic potential well. With technological advancements ultracold atoms can now be obtained in double well (DW) potential as well [25]. DW potential helps us to explore some wonderful properties of cold atoms like Josephson effects [26] and matter wave interference [27]. In a rotating trap the vortices and vortex lattices are formed depending on the speed of rotation. The Feynman rule says that the total number of vortices N_v increases linearly with the angular frequency of rotation Ω [28]. For an atomic BEC trapped in DW potential Feynman rule has been verified considering the hidden vortices along the central barrier of the trap together with the core vortices [29, 30]. Though these hidden vortices do not exist in density distribution of the atomic condensate give rise to phase singularities along the central barrier and appear in the density distribution after free expansion of the condensate [29]. Hidden vortices in dipolar atomic BECs in rotating DW trap has also been explored [31]. Hidden vorticity has also been studied considering binary BECs described by 2D Gross-Pitaevskii equations [32]. Enhancement in the vortex number by introducing artificial gauge potential in a condensate confined in DW potential has been examined [33].

The motivation of our present work is to study the dependence of the structure of vortex lattices formed in the coupled atomic-molecular BECs in a rotating DW trap on the variation of different system parameters e.g. atom-molecular coupling strength, Raman detuning and the frequency of rotation of the trap,

which has not been explored in detail to the best of our knowledge. We have considered two-photon Raman photo-association method for the coherent atomic to molecular formation in BEC. To investigate the effect of variation of different system parameters as mentioned above on the vortex lattice formation we carry out a numerical analysis of the coupled Gross-Pitaevskii equations considering rotating DW trap following Crank-Nicholson method. We analyzed how the variation of atom-molecular coupling strength, rotation frequency of the trap and the Raman detuning affects the structure of atomic and molecular vortex lattices, in particular the number of atomic and molecular vortices and the overlapping of atomic and molecular vortices in the lattice. The presence of atomic as well as molecular hidden vortices along the central barrier of rotating DW trap are clearly visible in the phase distribution and this hidden vortices have also been revealed in the density distributions when the DW trap is released and condensates are freely expanded. The Feynman rule of vortices is found to be satisfied well only after the inclusion of hidden atomic and molecular vortices along with the visible ones except in the cases where adjacent molecular vortices overlap with each other. It is found that although the number of visible vortices changes significantly with the variation of system parameters the number of hidden vortices remains unaffected in most of the cases.

In the next section 2, our theoretical model is formulated which describes the coupled atomic-molecular condensates in a rotating DW trap. Results of the numerical analysis have been presented in sections 3.1, 3.2 and 3.3 to discuss the effects of variation of (i) atom-molecule coupling strength, (ii) rotation frequency and the (iii) Raman detuning, respectively. Finally we conclude in section 4.

2 Theoretical model

The model system considered here is shown schematically in Fig. 1 which is also described in Ref. [7, 9]. The two atoms trapped in a DW potential in the atomic BEC state ($|a\rangle$) with total energy $2E_1$ form a molecular ground state $|g\rangle$ of energy E_2 via a rovibrational level $|v\rangle$ of energy E_v of an excited electronic state by two-photon Raman photoassociation. Levels $|a\rangle$ and $|v\rangle$ are coupled by a laser field with frequency ω_u and the levels $|v\rangle$ and $|g\rangle$ are coupled by a laser field with frequency ω_d . The process of Raman coupling becomes resonant when the two-photon Raman detuning $\epsilon = (2E_1 - E_2)/\hbar - (\omega_d - \omega_u)$ is zero. Both the atomic and the molecular condensate wave functions in the DW trap satisfy the coupled Gross-Pitaevskii (GP) equations with a Raman coupling constant χ .

Atomic and molecular BECs trapped in an external potential is described by the macroscopic wave functions $\psi_a(\mathbf{r}, \mathbf{t})$ and $\psi_m(\mathbf{r}, \mathbf{t})$ and the corresponding mean field energy density for the system in the rotating frame with frequency of rotation Ω may be given as

$$\begin{aligned}
E[\psi_a, \psi_m] = & \psi_a^* \left[-\frac{\hbar^2 \nabla^2}{2m} - \Omega L_z + V_a(\mathbf{r}) + \frac{\lambda_{aa}}{2} \psi_a^* \psi_a \right] \psi_a + \\
& \psi_m^* \left[-\frac{\hbar^2 \nabla^2}{4m} - \Omega L_z + V_m(\mathbf{r}) + \epsilon + \frac{\lambda_{mm}}{2} \psi_m^* \psi_m \right] \psi_m + \\
& \lambda_{am} \psi_a^* \psi_a \psi_m^* \psi_m + \frac{\chi}{2} [\psi_m^* \psi_a \psi_a + \psi_m \psi_a^* \psi_m^*]
\end{aligned} \tag{1}$$

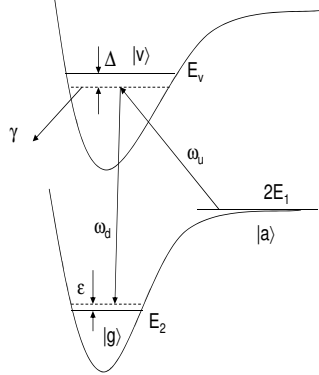


Figure 1: Schematic representation of Raman photoassociation

where λ_{aa} , λ_{mm} and λ_{am} represent the atom-atom, molecule-molecule and atom-molecule interactions, respectively. χ represents the strength of coupling between atoms and molecules due to stimulated Raman transitions and ϵ characterizes Raman detuning. $L_z = i\hbar(y\frac{\partial}{\partial x} - x\frac{\partial}{\partial y})$ is the z-component of angular momentum. Here the system of coupled condensates is considered to be in an axially symmetric trap ($\omega_x = \omega_y = \omega_{\perp}$) which is very strongly axial so that $\omega_x, \omega_y \ll \omega_z$ i.e. the trap is effectively two dimensional. The DW potential traps for atoms and molecules are given by

$$V_a(\mathbf{r}) = V_a(x, y) = \frac{1}{2}m\omega_{\perp}^2(x^2 + \lambda^2 y^2) + V_0 e^{-\frac{x^2}{2\sigma^2}} \quad (2)$$

and

$$V_m(\mathbf{r}) = V_m(x, y) = m\omega_{\perp}^2(x^2 + \lambda^2 y^2) + V_0 e^{-\frac{x^2}{2\sigma^2}} \quad (3)$$

where V_0 and σ denote the depth and width of the DW potential barrier, respectively. $\lambda = \frac{\omega_y}{\omega_x}$ is the anisotropy parameter of the trap.

At very low temperature the ground state of the system is described by the coupled Gross-Pitaevskii (GP) equations given by

$$i\hbar \frac{\partial \psi_a}{\partial t} = \frac{\delta E}{\delta \psi_a^*} \quad (4)$$

and

$$i\hbar \frac{\partial \psi_m}{\partial t} = \frac{\delta E}{\delta \psi_m^*} \quad (5)$$

Using the energy density given in Eq.(1) the coupled GP equations (4) and (5) take the following form:

$$i\hbar \frac{\partial \psi_a}{\partial t} = \left[-\frac{\hbar^2 \nabla^2}{2m} - \Omega L_z + V_a(x, y) + \lambda_{aa} |\psi_a|^2 + \lambda_{am} |\psi_m|^2 \right] \psi_a + \chi \psi_m \psi_a^* \quad (6)$$

$$i\hbar \frac{\partial \psi_m}{\partial t} = \left[-\frac{\hbar^2 \nabla^2}{4m} - \Omega L_z + V_m(x, y) + \epsilon + \lambda_{mm} |\psi_m|^2 + \lambda_{am} |\psi_a|^2 \right] \psi_m + \frac{\chi}{2} \psi_a^2 \quad (7)$$

As the trap is strongly axial ($\omega_x, \omega_y \ll \omega_z$) the system is reduced to effectively two-dimensional x-y space by taking the atomic and molecular wave functions as $\psi_a(\mathbf{r}) = \psi_a(z)\psi_a(x, y)$ and $\psi_m(\mathbf{r}) = \psi_m(z)\psi_m(x, y)$. $\psi_a(z)$ and $\psi_m(z)$ are taken as normalized Gaussian functions as: $\psi_{a,m}(z) = \frac{1}{(\pi d_z^2)^{1/4}} e^{\frac{-z^2}{2d_z^2}}$ where $d_z = \sqrt{\frac{\omega_\perp}{\omega_z}}$.

In order to reduce the equations (6) and (7) in dimensionless form the length and time are scaled as $x = a_h x_1$, $y = a_h y_1$ and $t = t_1/w_\perp$ with $a_h = \sqrt{\frac{\hbar}{2m w_\perp}}$. To include the effect of dissipation in vortex dynamics which may be due to the loss of atoms and molecules from the trap resulting from inelastic collisions the term $-\gamma \frac{\partial \psi_{a,m}}{\partial t}$ is added in equations (6) and (7) where γ is a dimensionless parameter characterizing the dissipation. Then the coupled equations (6) and (7) are reduced to the dimensionless form

$$(i - \gamma) \frac{\partial \psi_a}{\partial t} = \left[-\left(\frac{d^2}{dx_1^2} + \frac{d^2}{dy_1^2} \right) - i\Omega_1 (y_1 \frac{\partial}{\partial x_1} - x_1 \frac{\partial}{\partial y_1}) + \frac{1}{4} (x_1^2 + y_1^2) + V_{01} e^{\frac{-x_1^2}{2\sigma_1^2}} + \lambda_{aa_1} \eta_1 |\psi_a|^2 + \lambda_{am_1} \eta_2 |\psi_m|^2 \right] \psi_a + \chi_1 \eta_3 \psi_m \psi_a^* \quad (8)$$

and

$$(i - \gamma) \frac{\partial \psi_m}{\partial t} = \left[-\frac{1}{2} \left(\frac{d^2}{dx_1^2} + \frac{d^2}{dy_1^2} \right) - i\Omega_1 (y_1 \frac{\partial}{\partial x_1} - x_1 \frac{\partial}{\partial y_1}) + \frac{1}{8} (x_1^2 + y_1^2) + V_{01} e^{\frac{-x_1^2}{2\sigma_1^2}} + \lambda_{mm_1} \eta_{1m} |\psi_m|^2 + \lambda_{am_1} \eta_{2m} |\psi_a|^2 + \epsilon_1 \right] \psi_m + \frac{\chi_1}{2} \eta_{3m} \psi_a^2 \quad (9)$$

where $\lambda_{aa_1} = \frac{\lambda_{aa}}{\hbar \omega_\perp}$, $\lambda_{mm_1} = \frac{\lambda_{mm}}{\hbar \omega_\perp}$, $\lambda_{am_1} = \frac{\lambda_{am}}{\hbar \omega_\perp}$, $\chi_1 = \frac{\chi}{\hbar \omega_\perp}$, $\epsilon_1 = \frac{\epsilon}{\hbar \omega_\perp}$, $\Omega_1 = \frac{\Omega}{\hbar \omega_\perp}$, and

$$\eta_1 = \int \frac{|\psi_a(z)|^4 dz}{|\psi_a(z)|^2 dz} \quad (10)$$

$$\eta_2 = \int \frac{|\psi_m(z)|^2 |\psi_a(z)|^2 dz}{|\psi_a(z)|^2 dz} \quad (11)$$

$$\eta_3 = \int \frac{\psi_m(z) \{\psi_a^*(z)\}^2 dz}{|\psi_a(z)|^2 dz} \quad (12)$$

$$\eta_{1m} = \int \frac{|\psi_m(z)|^4 dz}{|\psi_m(z)|^2 dz} \quad (13)$$

$$\eta_{2m} = \int \frac{|\psi_a(z)|^2 |\psi_m(z)|^2 dz}{|\psi_m(z)|^2 dz} \quad (14)$$

$$\eta_{3m} = \int \frac{\psi_m^*(z) \{\psi_a(z)\}^2 dz}{|\psi_m(z)|^2 dz} \quad (15)$$

The normalization of the atomic and molecular wave functions can be given by the condition

$$|\psi_a(x, y)|^2 + 2|\psi_m(x, y)|^2 = 1 \quad (16)$$

In the following section we study the vortices of a coupled atomic-molecular BEC by solving the equations (8) and (9) with the help of Crank-Nicolson scheme [9, 10]. The iteration in time has been started with the initial atomic wave function taken as the normalized ground state solution of GP equation for atomic BEC in DW potential for $\Omega_1=0$ which can be written as

$$[-(\frac{d^2}{dx_1^2} + \frac{d^2}{dy_1^2}) + \frac{1}{4}(x_1^2 + y_1^2) + V_{01}e^{\frac{-x_1^2}{2\sigma_1^2}} + \lambda_{a1}\eta_1|\psi_a|^2]\psi_a = \mu_1\psi_a \quad (17)$$

where μ_1 is the chemical potential in the units of $\hbar\omega_\perp$.

The energies corresponding to atomic-molecular scattering

$$E_{am} = \lambda_{am} \int d\mathbf{r} |\psi_a|^2 |\psi_m|^2 \quad (18)$$

The energies corresponding to atomic-molecular coupling

$$E_c = \frac{\chi}{2} \int d\mathbf{r} [\psi_a^* \psi_a^* \psi_m + \psi_m^* \psi_m^* \psi_a] \quad (19)$$

The energies corresponding to rotation

$$E_{rot} = (-\Omega) \int d\mathbf{r} [\psi_a^* L_z \psi_a + \psi_m^* L_z \psi_m] \quad (20)$$

3 Results and Discussion

We have carried out a detailed numerical analysis of the effect of relative strength of atom-molecular coherent coupling and the interspecies interaction, Raman detuning and the rotation frequency of the trap on the vortex lattice formation in the coupled atom-molecular BECs in DW potential. To start with we assume the presence of atomic BEC only (with no molecules) inside the DW trap by making $\lambda_{am1} = \lambda_{mm1} = \chi_1 = 0$ in absence of rotation and the ground state solution of the 2D GP equation [Eq. (17)] for atomic BEC of ^{87}Rb atoms trapped in DW potential has been found out considering $\Omega_1 = 0$ using the imaginary time propagation method [34]. This ground state wave functions were used as initial

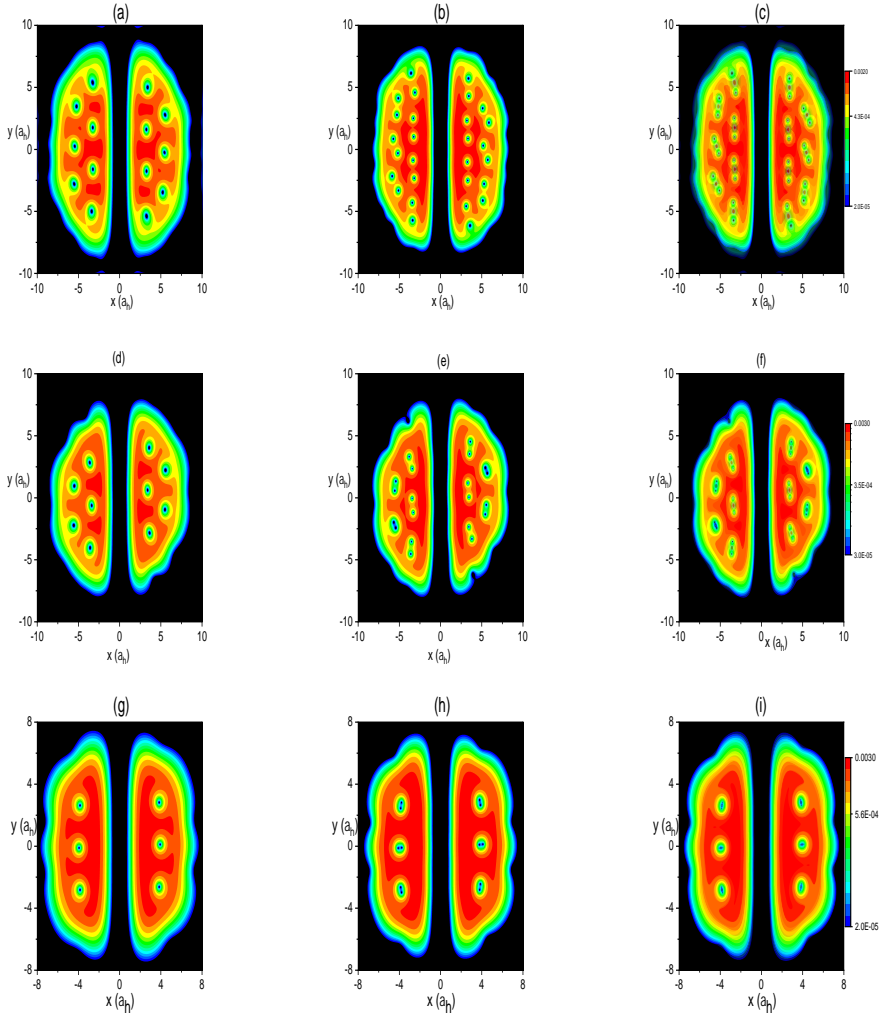


Figure 2: (Color online) Density distributions for atomic [Figs. (a), (d), (g)], molecular [Figs. (b), (e), (h)] and atomic with molecular [Figs. (c), (f), (i)] vortex lattice configuration for different coupling strengths $\chi_1 = 30$ [Figs. (a), (b), (c)], 50 [Figs. (d), (e), (f)] and 70 [Figs. (g), (h), (i)] at $t_1 = 300$. $\Omega_1 = 0.95$ and $\epsilon_1 = 0$. Red color corresponds to higher densities and blue color corresponds to lower densities. Darker color corresponds to lower density. x and y are in the units of $a_h = \sqrt{\frac{\hbar}{2m\omega_\perp}}$

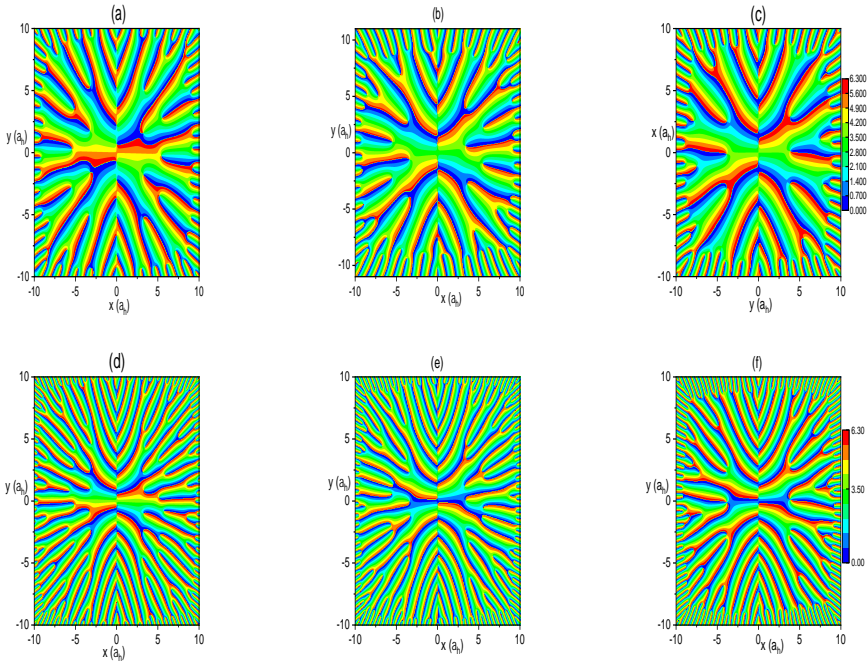


Figure 3: (Color online) Phase profile of atoms ψ_a for different coupling strengths $\chi_1 = 30$ [Fig. (a)], 50 [Fig. (b)] and 70 [Fig. (c)] and phase profile of molecules ψ_m for different coupling strengths $\chi_1 = 30$ [Fig. (d)], 50 [Fig. (e)] and 70 [Fig. (f)] at $t_1 = 300$. $\Omega_1 = 0.95$ and $\epsilon_1 = 0$. Phase varies from 0 to 2π . Red color corresponds to higher values and blue color corresponds to lower values. Darker color corresponds to lower phase. x and y are in the units of $a_h = \sqrt{\frac{\hbar}{2m\omega_{\perp}}}$.

wave functions to solve the 2D coupled atomic molecular GP equations [Eqs. (8) and (9)] with non zero values of Ω_1 by using Crank-Nicolson scheme [9, 10]. The space step and the time step are taken as $\Delta x = 0.05$ and $\Delta t = 0.0005$ respectively. The trap parameters are chosen as $\omega_x = \omega_y = \omega_{\perp} = 2\pi \times 40$ Hz, $\omega_z = 2\pi \times 800$ Hz, $V_0 = 40$ and $\sigma = 0.5$ as taken by Wen et al. [29]. We have taken $\lambda_{aa1} = 600$, $\lambda_{am1} = 0.85 \times \lambda_{aa1}$ (as considered by Woo et al. [23]), $\lambda_{mm1} = 2 \times \lambda_{aa1}$. Here we consider atom-atom, molecule-molecule and atom-molecule interactions to be repulsive. Ω_1 ranges from 0.85 to 0.95, χ_1 ranges from 30 to 70 and ϵ_1 ranges from -0.5 to 5. The initial value of χ_1 is so chosen that carbon-di-oxide like atomic-molecular vortex lattice structure could be obtained. The atom-atom, molecule-molecule and atom-molecule interactions have been kept fixed. The unit of length and time are $\sqrt{\frac{\hbar}{2m\omega_{\perp}}}$ and ω_{\perp}^{-1} respectively. The effect of dissipation is included by adding the term $-\gamma \frac{\partial \psi}{\partial t}$ in Eqs. (8) and (9). The value of γ is taken as 0.03 [29]. In this system three competing forces e.g. (i) atom-molecule repulsive interaction, (ii) atom-molecule coherent coupling strength which is attractive in this system and (iii) the centrifugal force from the rotation of the trap control the structure and the number of vortices in the vortex lattice of both atoms and molecules. The repulsive atom-molecule interaction energy tends to increase the distance between the atomic and molecular vortices whereas attractive atom-molecule coupling tends to reduce the distance between the atomic and molecular vortices. On the other hand increase in centrifugal forces due to the increase in rotation frequency leads to spread in density distribution effectively resulting in increase in the number of vortices. Conversely the decrease in rotation frequency tends to squeeze the atomic-molecular density distribution by restricting its spread which causes decrease in the number of vortices. Moreover it is found that the variation in the detuning ϵ_1 can also affect the nature of vortex lattice formation. It is found that the variation of any one of these parameters leads to variation in the overlap of the wave functions and hence leading to change in the energies. To explore these features of vortex lattice formation we have compared the three components of energies with variation of χ_1 , Ω_1 and ϵ_1 as presented in tables 1, 2 and 3, respectively.

3.1 Effect of variation of atom-molecule coupling strength on atom-molecular vortex lattices

In this section we study the effect of the change in atom-molecule coupling on the vortex lattice formation for a fixed value of rotation frequency ($\Omega_1 = 0.95$) and detuning ($\epsilon_1 = 0$). The vortex lattice structure of atoms, molecules and atoms with molecules for three different values of atom molecular coupling $\chi_1 = 30, 50$ and 70 , respectively is plotted in Fig.2. Density distributions for atoms ($|\psi_a|^2$), for molecules ($|\psi_m|^2$) and for atoms with molecules ($|\psi_a|^2$ and $|\psi_m|^2$) have been plotted in Figs. 2(a), 2(b) and 2(c), respectively for $\chi_1 = 30$. Similarly those for $\chi_1 = 50$ have been plotted in Figs. 2(d), 2(e) and 2(f) and for $\chi_1 = 70$ in Figs. 2(g), 2(h) and 2(i), respectively. These figures have been plotted as functions of x and y at $t_1 = 300$ as this is the time at which the wave functions become stable. By comparing atomic vortex lattices (Fig. 2(a), Fig. 2(d) and Fig. 2(g)) for $\chi_1 = 30, 50, 70$ it is found that the number of atomic vortices decreases with increase in the strength of atom-molecular coupling and the number of visible atomic vortices are 14, 10 and 6, respectively. However with the increase in

atom-molecular coupling strength both the distance between pair of molecular vortices as well as the number of molecular vortices decreases (Fig. 2(b), Fig. 2(e) and Fig. 2(h)) and the total number of visible molecular vortices are 28, 20 and 12 for $\chi_1 = 30, 50$ and 70 , respectively. This indicates that the density of molecular vortices is twice the density of atomic vortices which satisfies the relation that density of vortices is proportional to the mass of the constituent particles as given by Feynman [28]. By comparing the vortex lattices for atoms and molecules combined (Figs. 2(c), 2(f) and 2(i)) it is found that initially for $\chi_1=30$ (Fig. 2(c)) vortices (atoms and molecules) are arranged as CO_2 like structure, two molecular vortices are on the two opposite sides of atomic vortices. However with increase in the coupling strength (χ_1) the distance between atomic and molecular vortices decreases (Fig. 2(f)) and for the highest value of $\chi_1= 70$, both the atomic and molecular vortices almost overlap (Fig. 2(i)). Hence the variation of atom-molecular coupling strength controls the vortex lattice structure significantly by changing the distance between atomic and molecular vortices as well as the total number of vortices. To explore the physics behind the effect of variation of atom-molecular coupling strength on the vortex lattice structure we have analyzed the dependence of vortex lattice formation on the energy components of the coupled system, (i) energies corresponding to atom-molecule coupling E_c , (ii) atom-molecular interaction energy E_{am} and (iii) the rotational energy E_{rot} and the values of these three energies have been given in Table-1 for three different values of χ_1 (30, 50 and 70). Atom-atom and molecule-molecule interaction energies are not tabulated as these are lower than E_c , E_{am} and E_{rot} by few orders of magnitude. From Table-1 it is found that as χ_1 increases, the attractive coupling energy E_c dominates over the atom-molecular repulsive energy E_{am} and hence the ratio $|E_c/E_{am}|$ increases. In this system the attractive interaction E_c leads to decrease in the distance between atomic and molecular vortices effectively squeezing the molecular vortices towards the atomic vortices, whereas repulsive atom-molecular interaction leads to increase in the distance between atomic molecular vortices effectively pushing the molecular vortices away from the atomic vortices. Hence the interplay between these two forces determine the distance between atomic and molecular vortices. Therefore as the coupling energy E_c increases and dominates over E_{am} , the distance between atomic and molecular vortices as a result that between molecular vortices decreases and finally overlaps as shown in Fig 2. In Table- 1, the rotational energy has been found to decrease with the increase in the value of χ_1 . Although the rotational frequency remains the same the variation in the parameter χ_1 leads to variation in the wave functions of the system leading to the decrease in the rotational energy. Decrease in rotational energy restricts the spread of the lattices and hence leads to decrease in the number of vortices as it is evident from Fig. 2.

Furthermore this result is supported by the nature of variation of atomic and molecular angular momentum l_z per atom (or molecule) averaged over the whole condensate which is given as follows.

$$l_z = \frac{\int \psi^* L_z \psi dx dy}{\int |\psi|^2 dx dy} \quad (21)$$

It is found that with increase in χ_1 , l_z for both atoms and molecules decreases. Hence the number of vortices in the lattice decreases. However in each case, l_z is found to be much greater than the half of visible number of atomic and

Table 1: Comparison between different components of energies for three different values of χ_1 , $\Omega_1 = 0.95$ and $\epsilon_1 = 0$. Energies are in the units of $\hbar\omega_{\perp}$.

	E_c	E_{am}	$ E_c/E_{am} $	$ E_{rot} $
$\chi_1=30$	-0.142	0.111	1.280	5.050
$\chi_1=50$	-0.303	0.133	2.278	4.149
$\chi_1=70$	-0.382	0.116	3.293	2.772

molecular vortices. Here values of atomic (molecular) l_z for $\chi_1 = 30, 50$ and 70 are 14 (26), 12 (23) and 10 (19), respectively. However from vortex lattices shown in Figs. 2(a), 2(b), 2(d), 2(e), 2(g) and 2(h) for $\chi_1 = 30, 50$ and 70 the number of visible atomic and molecular vortices are $N_{v,a}$ ($N_{v,m}$)= 14 (28), 10 (20) and 6 (12), respectively. According to Feynman's rule l_z should be $N_v/2$ where N_v is the total number of vortices. Hence the Feynman's rule is apparently violated here. To investigate this disparity we have calculated the corresponding atomic and molecular phase distributions from the final stable wave functions $\psi_a(x, y)$ and $\psi_m(x, y)$ and the phase varies from 0 to 2π . The corresponding atomic and molecular phase profiles are plotted in Fig. 3. It is evident from the phase distribution that there are some phase singularities in the central barrier region of the trap other than the position of visible vortices. If $N_{h,a}$ and $N_{h,m}$ are the total number of phase singularities corresponding to the atomic and molecular hidden vortices then from Figs. 2(a), 2(b), 3(a) and 3(b) for $\chi_1 = 30$: l_z (atomic) = $(N_{v,a}+N_{h,a})/2 = (14+14)/2 = 14$ and l_z (molecular) = $(N_{v,m}+N_{h,m})/2 = (28+24)/2 = 26$. Similarly from Figs. 2(d), 2(e), 3(c) and 3(d) for $\chi_1 = 50$: l_z (atomic) = $(N_{v,a}+N_{h,a})/2 = (10+14)/2 = 12$ and l_z (molecular) = $(N_{v,m}+N_{h,m})/2 = (20+26)/2 = 23$. And from Figs. 2(g), 2(h), 3(e) and 3(f) for $\chi_1 = 70$: l_z (atomic) = $(N_{v,a}+N_{h,a})/2 = (6+14)/2 = 10$ and l_z (molecular) = $(N_{v,m}+N_{h,m})/2 = (12+26)/2 = 19$.

This indicates that the hidden vortices carry the angular momentum just like the visible vortices. Fig. 3 shows that the number of atomic and molecular hidden vortices remain nearly constant with the variation in χ_1 unlike the visible vortices for which the number diminishes with the increase in χ_1 . This may be due to the fact that the magnitude of the atomic and molecular wave functions in the forbidden region (the central barrier) is much less than that within the trap. Hence the change in the overlap of the wave functions in the forbidden region becomes less effective to cause prominent change in the energy components mentioned above. Atomic and molecular condensates are expanded freely for $t_1 = 1$ and the density and the phase distributions for $\chi_1 = 30$ and 50 , for $\Omega_1 = 0.95$ and $\epsilon_1 = 0$ are plotted in Fig. 4. These figures reveal that free expansion make a couple of new vortices visible along the symmetry axis of the trap which are otherwise invisible. These new visible vortices must have been originated from hidden vortices which are evident in phase singularities.

Table 2: Comparison between different components of energies for two different values of Ω_1 , $\chi_1 = 30$ and $\epsilon_1 = 0$, Energies are in the units of $\hbar\omega_{\perp}$.

	E_c	$E_{a,m}$	$ E_c/E_{a,m} $	$ E_{rot} $
$\Omega_1 = 0.85$	-0.278	0.304	0.914	2.663
$\Omega_1 = 0.9$	-0.211	0.209	1.009	4.127
$\Omega_1 = 0.94$	-0.161	0.134	1.201	4.893
$\Omega_1 = 0.95$	-0.142	0.111	1.279	5.050

Table 3: Comparison between different components of energies for three different values of ϵ_1 , $\Omega_1 = 0.95$ and $\chi_1 = 50$. Energies are in the units of $\hbar\omega_{\perp}$.

	E_c	$E_{a,m}$	$ E_c/E_{a,m} $	$ E_{rot} $
$\epsilon_1 = -0.5$	-0.298	0.148	2.013	3.194
$\epsilon_1 = 0$	-0.303	0.133	2.278	4.149
$\epsilon_1 = 2$	-0.306	0.101	3.029	4.882
$\epsilon_1 = 5$	-0.309	0.082	3.768	5.134

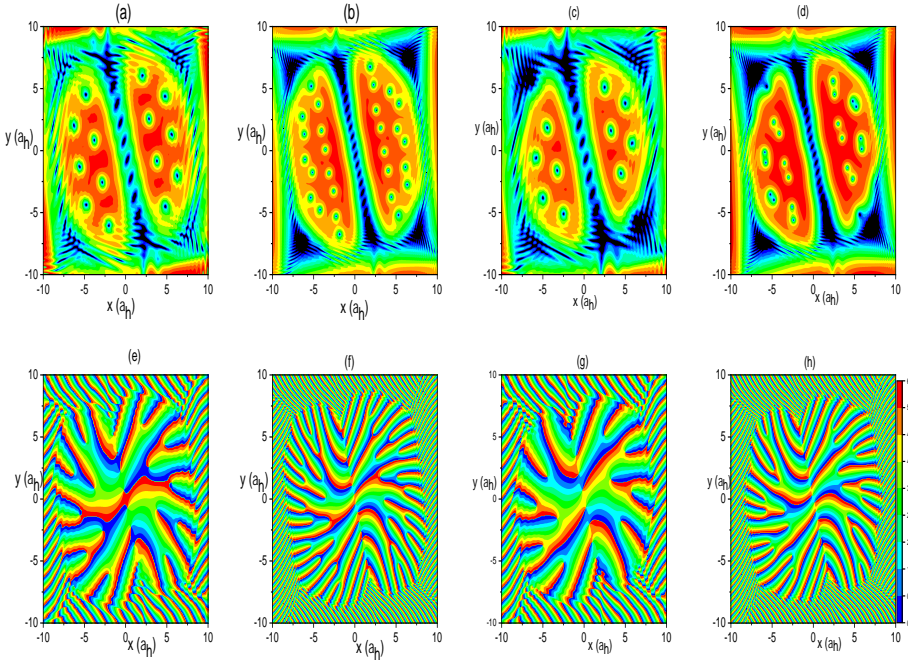


Figure 4: (Color online) Density distribution of atomic [Figs. (a), (c)] and molecular [Figs. (b), (d)] condensate along with phase profile of ψ_a [Figs. (e), (g)] and ψ_m [Figs. (f), (h)] after free expansion for $t_1 = 1$. The corresponding parameters are $\Omega_1 = 0.95$, $\epsilon_1 = 0$ and $\chi_1 = 30$ [Figs. (a), (b), (e), (f)] and 50 [Figs. (c), (d), (g), (h)]. Red color corresponds to higher values and blue color corresponds to lower values. Darker color corresponds to lower density. x and y are in the units of $a_h = \sqrt{\frac{\hbar}{2m\omega_\perp}}$.

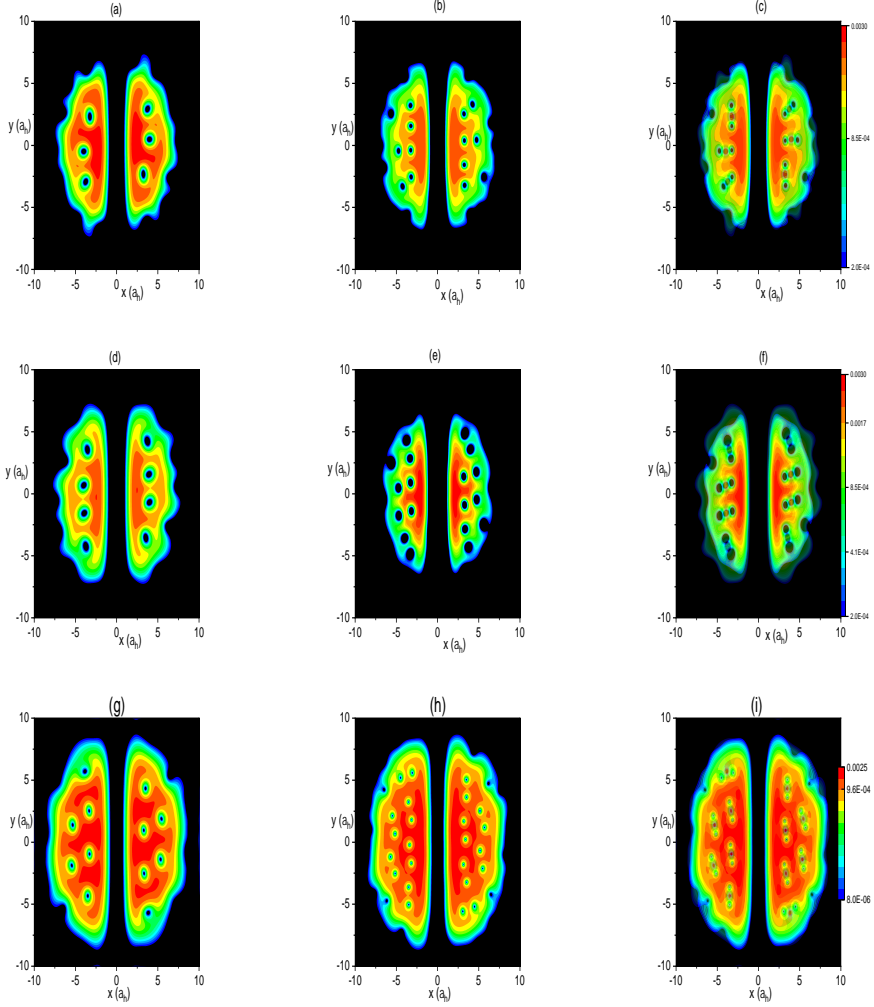


Figure 5: (Color online) Density distributions for atomic [Figs. (a), (d), (g)], molecular [Figs. (b), (e), (h)] and atomic with molecular [Figs. (c), (f), (i)] vortex lattice configurations for different rotation frequencies $\Omega_1 = 0.85$ [Figs. (a), (b), (c)] , 0.9 [Figs. (d), (e), (f)] and 0.94 [Figs. (g), (h), (i)] at $t_1 = 300$. $\chi_1 = 30$ and $\epsilon_1 = 0$. Red color corresponds to higher densities and blue color corresponds to lower densities. Darker color corresponds to lower density. x and y are in the units of $a_h = \sqrt{\frac{\hbar}{2m\omega_\perp}}$.

3.2 Effect of variation of rotational frequency on atom-molecular vortex lattices

To study the effect of variation of rotational frequency (Ω_1) on the vortex lattice structure we consider the fixed values of atom-molecule coupling strength ($\chi_1 = 30$) and detuning ($\epsilon_1 = 0$). We varied the rotational frequency (Ω_1) from values 0.85 to 0.95 to examine its effect on the atomic-molecular vortex lattice structure and plotted the atomic and molecular densities as functions of x and y in Fig. 5. Previously in Figs. 2(a) and 2(b) we have shown the vortex lattice formed for $\Omega_1 = 0.95$, $\chi_1 = 30$ and $\epsilon_1 = 0$. In Fig. 5 we have plotted the vortex lattices for atoms and molecules for the values of $\Omega_1 = 0.85, 0.90$ and 0.94 . Figs. 5(a), 5(d) and 5(g) show the atomic vortex lattices and Figs. 5(b), 5(e) and 5(h) show the molecular vortex lattices for $\Omega_1 = 0.85, 0.90$ and 0.94 , respectively. Combined vortex lattices for atoms with molecules are shown in Figs. 5(c), 5(f) and 5(i) for values of $\Omega_1 = 0.85, 0.90$ and 0.94 , respectively. Corresponding phase profiles for atoms and molecules are plotted in Fig. 6 for $\Omega_1 = 0.9$. It is found that the number of atomic and molecular vortices increases with the increase in rotational frequency. With the increase in rotational frequency the centrifugal force increases and it forces the condensate to spread more towards the edges of the trap. The corresponding energy components are given in Table-2. From Table-2 it is found that with the increase in rotational frequency the rotational energy increases leading to increase in the number of atomic and molecular vortices. However the values of $|E_c/E_{a,m}|$ increase by very small amount on the increase in Ω_1 and hence there is no significant change in the relative distance between atomic and molecular vortices. Numerically calculated values of l_z (atomic) and l_z (molecular) are 11 and 20 respectively for $\Omega_1 = 0.9$. Whereas the number of real atomic ($N_{v,a}$) and molecular ($N_{v,m}$) vortices are 8 and 16 [from Figs. 5(d) and 5(e)]. From the corresponding phase distribution of ψ_a and ψ_m plotted in Figs. 6(a) and 6(b), the number of hidden atomic ($N_{h,a}$) and molecular ($N_{h,m}$) vortices are 14 and 24. This satisfies the Feynman rule l_z (atomic) = $(N_{v,a} + N_{h,a})/2 = (8+14)/2 = 11$ and l_z (molecular) = $(N_{v,m} + N_{h,m})/2 = (16+24)/2 = 20$. Previously in section 3.1 we have shown that Feynman rule is satisfied for $\Omega_1 = 0.95$ by considering both the visible and hidden vortices. We have also found that Feynman rule is well satisfied (results are not shown here) for other values of Ω_1 considered here.

3.3 Effect of variation of detuning on atom-molecular vortex lattices

In order to study the effect of variation of Raman detuning parameter ϵ_1 on the formation of atomic and molecular vortex lattices the density profiles for atoms ($|\psi_a|^2$), for molecules ($|\psi_m|^2$) and for atom and molecule combined ($|\psi_a|^2$ with $|\psi_m|^2$) are plotted as functions of x and y in Fig. 7 for three different values of Raman detuning $\epsilon_1 = -0.5, 2$ and 5 , keeping χ_1 and Ω_1 fixed at 50 and 0.95. Figs. 7(a), 7(d) and 7(g) show atomic lattices, Figs. 7(b), 7(e) and 7(h) show molecular lattices and Figs. 7(c), 7(f) and 7(i) show lattices for atomic-molecular vortices combined for three values of detuning $\epsilon_1 = -0.5, 2$ and 5 , respectively. It is found that the number of visible atomic (Figs. 7(a), 7(d) and 7(g)) and molecular (Figs. 7(b), 7(e) and 7(h)) vortices are 6 and 12 for $\epsilon_1 = -0.5$, those are 14 and 28 for $\epsilon_1 = 2$, whereas those for $\epsilon_1 = 5$ are 18 and 36 respectively. From

Figs. 2(d) and 2(e) we find the number of visible atomic and molecular vortices are 10 and 20 respectively for $\epsilon_1 = 0$. By comparing results from Fig. 7 and Fig. 2 it is found that the number of atomic and molecular vortices increases gradually with the increase in detuning. Moreover if we compare the structure of molecular lattices (Figs. 7(b), 7(e), 7(h) and 2(e)) it is evident that the distance between molecular vortices gradually decreases with increase in detuning and finally completely superpose on each other and become indistinguishable. Hence two molecular vortices which were well separated for $\epsilon_1 = -0.5$ and 0 (Fig. 7(b) and Fig. 2(e)) approach towards each with further increase in detuning (Fig. 7(e)) and finally merge with each other (Fig. 7(h)). Since the atomic vortex is in between the two molecular vortices (Fig. 7(c)), with the increase in detuning two molecular vortices approach towards the atomic vortex and completely overlap with each other and also with the atomic vortex (Fig. 7(i)). Hence in the projection on the $x - y$ plane three overlapped vortices look like a single vortex. To analyze these two features of vortex lattices: (i) increase in the number of atomic and molecular vortices and (ii) decrease in the distance between atomic and molecular vortices leading to the decrease in distance between two molecular vortices with the increase in the detuning, corresponding energy components for $\epsilon_1 = -0.5, 0, 2$ and 5 are given in Table- 3. From Table- 3, we find that the rotational energy E_{rot} and the ratio of atom-molecular coupling energy and atom-molecular interaction energy $|E_c/E_{a,m}|$ both increase with ϵ_1 . The increase in the rotational energy gives rise to more spread of the condensate towards the edge of the trap leading to the increase in the number of visible vortices. Whereas increase in $|E_c/E_{a,m}|$ with the increase in ϵ_1 leads to squeezing of the vortices i.e. decrease in relative distance between atomic and molecular vortices leading to decrease in the relative distance between two molecular vortices. Hence the atomic and molecular vortices which are separated for $\epsilon_1 = -0.5$ (Fig. 7(c)) and 0 (Fig. 2(f)), tend to merge with increase in ϵ_1 [Fig. 7(f)] and finally they superpose on each other at $\epsilon_1 = 5$ (Fig. 7(i)). In Figs. 3(b) and 3(e) we have shown the phase distribution of ψ_a and ψ_m for $\epsilon_1 = 0$ (for $\chi_1 = 50$ and $\Omega_1 = 0.95$). In Fig. 8, we have plotted the phase distribution of ψ_a and ψ_m for $\epsilon_1 = -0.5$ (Figs. 8(a) and 8(b)), for $\epsilon_1 = 2$ (Figs. 8(c) and 8(d)) and for $\epsilon_1 = 5$ (Figs. 8(e) and 8(f)). In section 3.1 we have shown how the Feynman rule is satisfied for $\epsilon_1 = 0$ by considering hidden vortices (counting singularities along the central barrier region in phase distribution) with visible vortices (from the density distribution) both for atomic and molecular vortex lattices. Here values of atomic (molecular) l_z for $\epsilon_1 = -0.5, 2$ and 5 are 10 (19), 14 (24) and 16 (26), respectively. However from vortex lattices shown in Figs. 7(a), 7(b), 7(d), 7(e), 7(g) and 7(h) for $\epsilon_1 = -0.5, 2$ and 5 the number of visible atomic and molecular vortices are $N_{v,a}$ ($N_{v,m}$)= 6 (12), 14 (28) and 18 (36), respectively. If $N_{h,a}$ and $N_{h,m}$ are the total number of phase singularities corresponding to the atomic and molecular hidden vortices then from Fig. 8, $N_{h,a} = 14$ and $N_{h,m} = 26$ for all the detunings $\epsilon_1 = -0.5, 2$ and 5, respectively. Hence l_z (atomic) should be equal to $(N_{v,a} + N_{h,a})/2 = (6+14)/2 = 10$ and l_z (molecular) should be equal to $(N_{v,m} + N_{h,m})/2 = (12+26)/2 = 19$ for $\epsilon_1 = -0.5$. This shows Feynman rule is satisfied for both the atomic and molecular vortices for $\epsilon_1 = -0.5$. However for $\epsilon_1 = 2$ and 5 (from Figs. 7(d), 7(e), 8(c), 8(d), 7(g), 7(h), 8(e) and 8(f)) it is found that for atomic vortices $(N_{v,a} + N_{h,a})/2 = (14+14)/2 = 14$ and $(N_{v,a} + N_{h,a})/2 = (18+14)/2 = 16$, respectively whereas for molecular vortices $(N_{v,m} + N_{h,m})/2 = (28+26)/2 = 27$ and $(N_{v,m} + N_{h,m})/2 = (36+26)/2 = 31$, re-



Figure 6: (Color online) Phase profile of ψ_a [Fig. (a)] and ψ_m [Fig. (b)] for rotation frequency $\Omega_1 = 0.9$ with $\chi_1 = 30$ and $\epsilon_1 = 0$ at $t_1 = 300$. Red color corresponds to higher values and blue color corresponds to lower values. Darker color corresponds to lower phase. x and y are in the units of $a_h = \sqrt{\frac{\hbar}{2m\omega_{\perp}}}$.

spectively. Therefore we find that the Feynman's rule is well satisfied for atomic vortices for all the values of detuning considered here. However for molecular vortices although the Feynman's rule is satisfied for smaller values of detuning ($\epsilon_1 = -0.5$ and 0), it deviates for larger values of detuning ($\epsilon_1 = 2$ to 5) and the deviation from Feynman rule for molecular vortex lattice increases with increase in detuning. It is found from Figs. 7 that with increase in detuning from zero, carbon-dioxide type structure of atomic and molecular vortices is overwritten by overlapping of molecular vortices with each other as well as with the atomic vortices in the middle. The number of overlapping molecular vortices increases with increase in detuning ($\epsilon_1 = 2$ to 5) leading to increase in the disagreement of Feynman rule for molecular vortices. In the definition of average angular momentum [Eq.(21)] it is shown that calculation of l_z involves spatial integration. Therefore when the molecular vortices superpose on each other it becomes indistinguishable for integration over space, effectively leading to a lower value of l_z . As a result the discrepancy between value of l_z and half of the total number of vortices increases. However while counting the total number of molecular vortices, if the two superposed molecular vortices are counted as single molecular vortex effectively the difference between l_z and half of the total number of vortices reduces to be one or zero.

This is a new feature of molecular vortex lattices, that the dynamics of molecular vortices i.e. the distance between two molecular vortices can be controlled by varying the Raman detuning. This can be experimentally observed by in situ imaging [34] of molecular vortex lattices in atom molecular coupled BEC (which are coherently coupled by two-photon Raman photoassociation [35]) by varying the Raman detuning. When the Raman detuning is varied from lower to higher values the dynamics of molecular vortices i.e. approach of two molecular vortices towards each other and finally merging on each other to be indistinguishable in the molecular vortex lattices can be observed. Moreover in atom-molecular combined vortex lattice system one can observe that from CO_2 like structure of atomic with molecular vortices will start squeezing towards each other and finally three vortices will merge with the increase in Raman detuning.

4 Conclusions

In conclusion, we have studied in detail the atomic-molecular vortex lattice formation of a rotating BEC in a double well trap by numerically solving the two-dimensional coupled GP like equations. We considered two photon Raman photoassociation for atom to molecule conversion. We found that both the atomic and molecular vortices those are hidden in density distribution could be revealed in phase distribution and adding the number of hidden vortices (along the barrier of the double well trap potential) with the visible vortices in the trap the Feynman rule is satisfied in general, however for large detuning a deviation from the Feynman rule for molecular vortices is observed and this can be attributed to the structural change in the vortex lattice i.e. carbon-dioxide type structure is overwritten by overlapping of molecular vortices with atomic vortices in the middle and hence three overlapped vortices two molecular and one atomic appear to be a single vortex. The number of vortices in molecular BEC is always twice than that of atomic BEC as the mass of a molecule is twice of that of an atom and number of vortices is proportional to the constituent masses. We explored the dependence of vortex lattice structure on the system parameters such as relative strength of atom-molecular coupling and atom-molecular interaction, rotational frequency and the Raman detuning. Our investigation reveals that the competition between atom-molecular coupling strength and atom-molecular interaction controls the spacing between atomic and molecular vortices and the rotational energy controls the number of atomic and molecular vortices in the vortex lattices. When coupling overpowers atom-molecular scattering, distance between atomic and molecular vortices decreases and tends to overlap with each other. Whereas when the rotational energy increases it leads to increase in the spread of the lattices towards the edge of the trap as well as the number of vortices in the vortex lattices. The Raman detuning parameter also controls the coupled vortex system by changing the relative strength of atom-molecular coupling and atom-molecular interaction as well as rotational energy and hence it controls both the spacing between vortices and the number of vortices. To explain all the features obtained in vortex lattices by varying the system parameters such as relative strength of atom-molecular coupling and the atom molecular interaction, rotational frequency of the trap and the Raman detuning we have analyzed different energy components as a function of these parameters. It is found that although the energy components, angular momentum and number of visible vortices of the coupled condensates largely depend on the atom-molecule coupling, rotation frequency and Raman detuning, the number of atomic and molecular hidden vortices those are evident in the phase singularities along the central barrier region of the trap remains nearly unaffected by the variation of these parameters. Therefore this atomic-molecular vortex system in a rotating double well trap offers some effective tools to control the coupled vortex dynamics confining the system in the stability domain.

5 Acknowledgement

We thank Bimalendu Deb, School of Physics, Indian Association for the Cultivation of Science for his interest in this work.

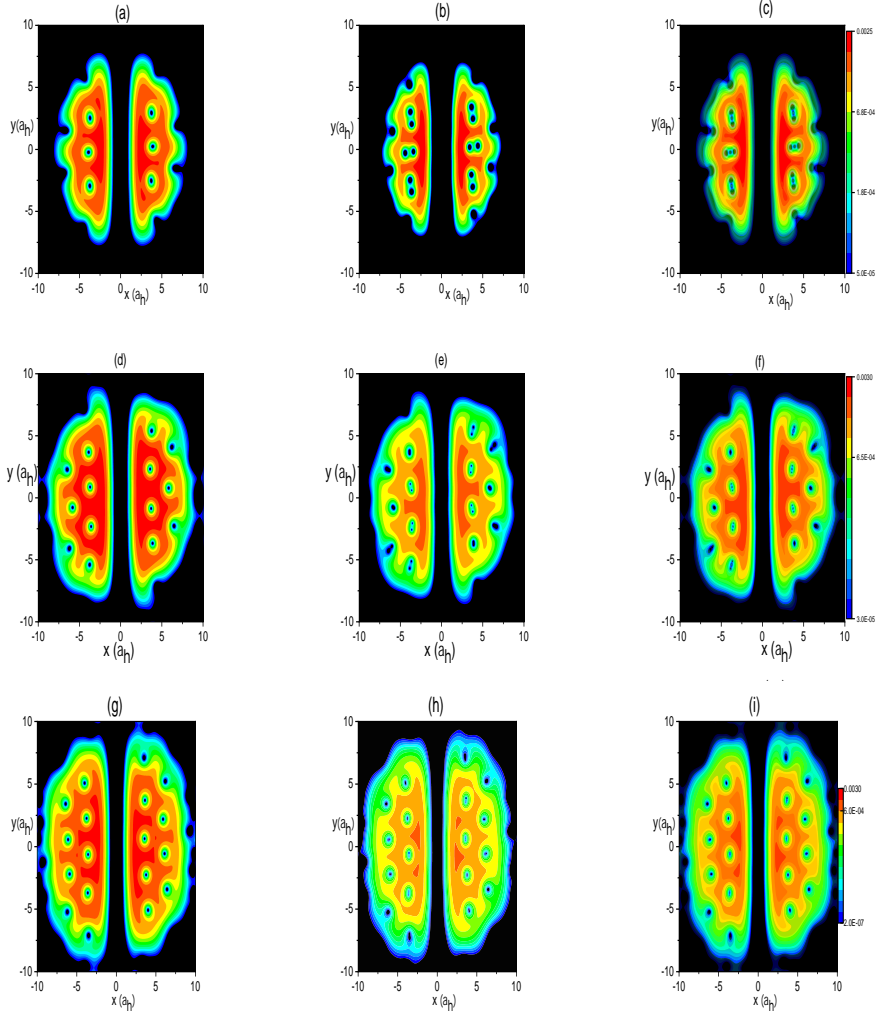


Figure 7: (Color online) Density distributions for atomic [Figs. (a), (d), (g)], molecular [Figs. (b), (e), (h)] and atomic with molecular [Figs. (c), (f), (i)] vortex lattice configuration for different detuning parameters $\epsilon_1 = -0.5$ [Figs. (a), (b), (c)], 2 [Figs. (d), (e), (f)] and 5 [Figs. (g), (h), (i)] at $t_1 = 300$. $\Omega_1 = 0.95$ and $\chi_1 = 50$. Red color corresponds to higher densities and blue color corresponds to lower densities. Darker color corresponds to lower density. x and y are in the units of $a_h = \sqrt{\frac{\hbar}{2m\omega_{\perp}}}$.

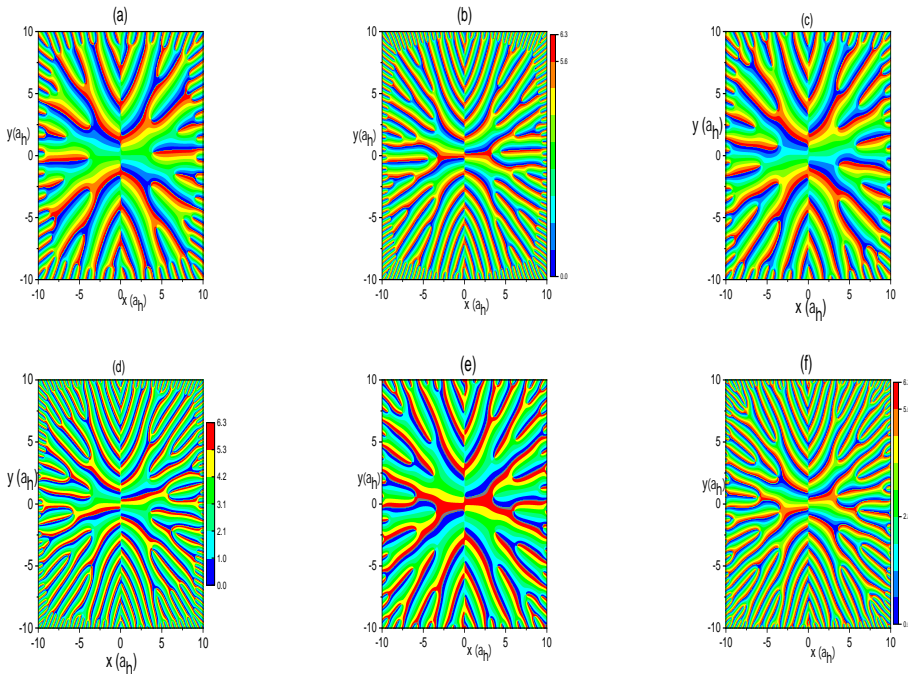


Figure 8: (Color online) Phase profile of atoms ψ_a for different detuning parameters $\epsilon_1 = -0.5$ [Fig. (a)], 2 [Fig. (c)], 5 [Fig. (e)] and phase profile of molecules ψ_m for different $\epsilon_1 = -0.5$ [Fig. (b)], 2 [Fig. (d)], 5 [Fig. (f)] at $t_1 = 300$. $\chi_1 = 50$ and $\epsilon_1 = 0$. Phase varies from 0 to 2π . Red color corresponds to higher values and blue color corresponds to lower values. Darker color corresponds to lower phase. x and y are in the units of $a_h = \sqrt{\frac{\hbar}{2m\omega_\perp}}$

References

- [1] R. Wynar, R. S. Freeland, D. J. Han, C. Ryu and D. J. Heinzen, *Science* **287**, 1016 (2000).
- [2] K. Winkler, F. Lang, G. Thalhammer, P. v. d. Straten, R. Grimm and J. H. Denschlag, *Phys. Rev. Lett.* **98**, 043201 (2007).
- [3] J. G. Danzl *et al.*, *Science* **321**, 1062 (2008)
- [4] S. T. Thompson, E. Hodby, and C. E. Wieman, *Phys. Rev. Lett.* **95**, 190404 (2005).
- [5] E. Timmermans *et al.*, *Phys. Rev. Lett.* **83**, 2691 (1999).
- [6] E. Timmermans *et al.*, *Phys. Rep.* **315**, 199 (1999).
- [7] D. J. Heinzen, R. Wynar, P. D. Drummond and K. V. Kheruntsyan, *Phys. Rev. Lett.* **84**, 5029 (2000).
- [8] F. D. de Oliveira and M. K. Olsen, *Opt. Comm.* **234**, 235 (2004).
- [9] M. Gupta and K. R. Dastidar, *Phys. Rev. A* **80**, 043618 (2009).
- [10] M. Gupta and K. R. Dastidar, *Phys. Rev. A* **81**, 033610 (2010).
- [11] J. J. Hope and M. K. Olsen, *Phys. Rev. Lett.* **86**, 3220 (2001).
- [12] K. W. Madison, F. Chevy, W. Wohlleben and J. Dalibard, *Phys. Rev. Lett.* **84**, 806 (2000).
- [13] J. R. Abo-Shaeer, C. Raman, J. M. Vogels, and W. Ketterle *Science* **292**, 476 (2001).
- [14] M. Tsubota, K. Kasamatsu, and M. Ueda *Phys. Rev. A* **65**, 023603 (2002).
- [15] K. Kasamatsu, M. Tsubota, and M. Ueda *Phys. Rev. A* **67**, 033610 (2003).
- [16] R. Kishor Kumar and P. Muruganandam *J. Phys. B: At. Mol. Opt. Phys.* **45**, 215301 (2012).
- [17] R. Kishor Kumar, T. Sriraman, H. Fabreli, P. Muruganandam and A. Gammal *J. Phys. B: At. Mol. Opt. Phys.* **49**, 155301 (2016).
- [18] Lin-Xue Wang, B. Dong, Guang-Ping Chen, W. Han, Shou-Gang Zhang, Yu-Ren Shi, and Xiao-Fei Zhang *Phys. Lett. A* **380**, 435 (2016) (DOI:).
- [19] R. Kishor Kumar, A. gammal, and L. Tomio *Phys. Lett. A* **384**, 126535 (2020).
- [20] S. Dutta, K. R. Dastidar, and C. Chaudhuri *J. Phys. B: At. Mol. Opt. Phys.* **53**, 065303 (2020).

- [21] K. Kasamatsu, M. Tsubota, and M. Ueda *Phys. Rev. Lett.* **93**, 250406 (2004).
- [22] M. Nitta, M. Eto, and M. Cipriani *J. Low Temp. Phys.* **175**, 177 (2014).
- [23] S. J. Woo, Q-Han Park, and N. P. Bigelow, *Phys. Rev. Lett.* **100**, 120403 (2008).
- [24] Chao-Fei Liu, H. Fan, Shih-Chuan Gou, and Wu-Ming Liu, *Scientific Reports* **4**, 4224 (2014).
- [25] M. Albiez, R. Gati, J. Folling, S. Hunsmann, M. Cristiani, and M. K. Oberthaler, *Phys. Rev. Lett.* **95**, 010402 (2005); S. Hofferberth, I. Lesanovsky, B. Fischer, T. Schumm, and J. Schmiedmayer, *Nature (London)* **449**, 324 (2007); J. Est‘eve, C. Gross, A. Weller, S. Giovanazzi, and M. K. Oberthaler, *Nature (London)* **455**, 1216 (2008); A. Weller, J. P. Ronzheimer, C. Gross, J. Esteve, M. K. Oberthaler, D. J. Frantzeskakis, G. Theocharis, and P. G. Kevrekidis, *Phys. Rev. Lett.* **101**, 130401 (2008).
- [26] S. Levy, E. Lahoud, I. Shomrani, and J. Steinhauer *Nature* **449**, 579 (2007).
- [27] M. Andrews et al. *Science* **275**, 637 (1997).
- [28] R. P. Feynman *Prog. Low Temp. Phys.* **1**, 17 (1955).
- [29] L. Wen, H. Xiong, and B. Wu *Phys. Rev. A* **82**, 053627 (2010).
- [30] T. Mithun, K. Porsezian, and B. Dey *Phys. Rev. A* **89**, 053625 (2014).
- [31] S. Subramaniyan *Phys. Lett. A* **381**, 3062 (2017).
- [32] M. Brtka, A. Gammal, and B. A. Malomed *Phys. Rev. A* **82**, 053610 (2010).
- [33] R. Bai, A. Roya, D. Angom, and P. Muruganandam *Phys. Lett. A* **382**, 2376 (2018).
- [34] K. E. Wilson, Z. L. Newman, J. D. Lowney, and B. P. Anderson *Phys. Rev. A* **91**, 023621 (2015).
- [35] E. A. Donley, N. R. Claussen, S. T. Thompson and C. E. Wieman, *Nature* **417**, 529 (2002).